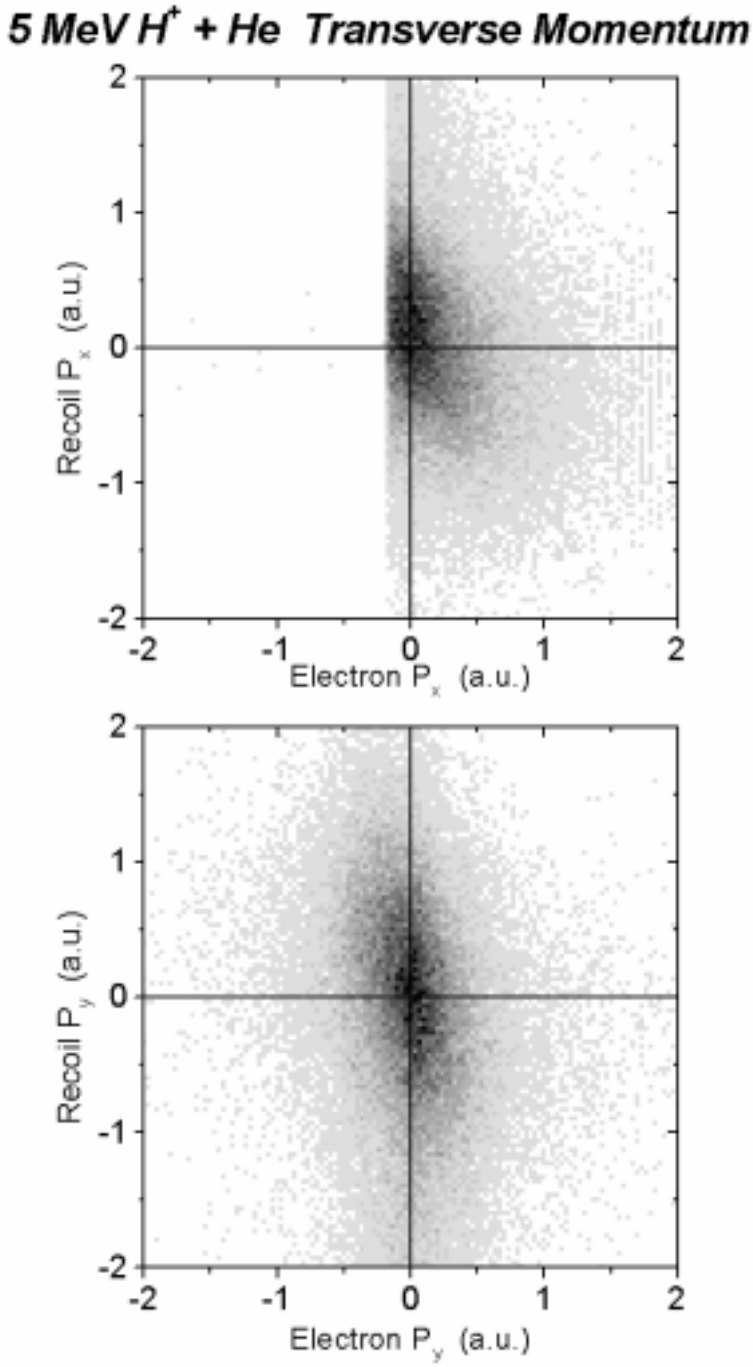

Figure 4.16: Density plots of the doubly differential cross sections $d^2\sigma/dP_{xe}\,dP_{xR}$ and $d^2\sigma/dP_{yR}\,dP_{ye}$ for the collision system 5 MeV H^+ + He.

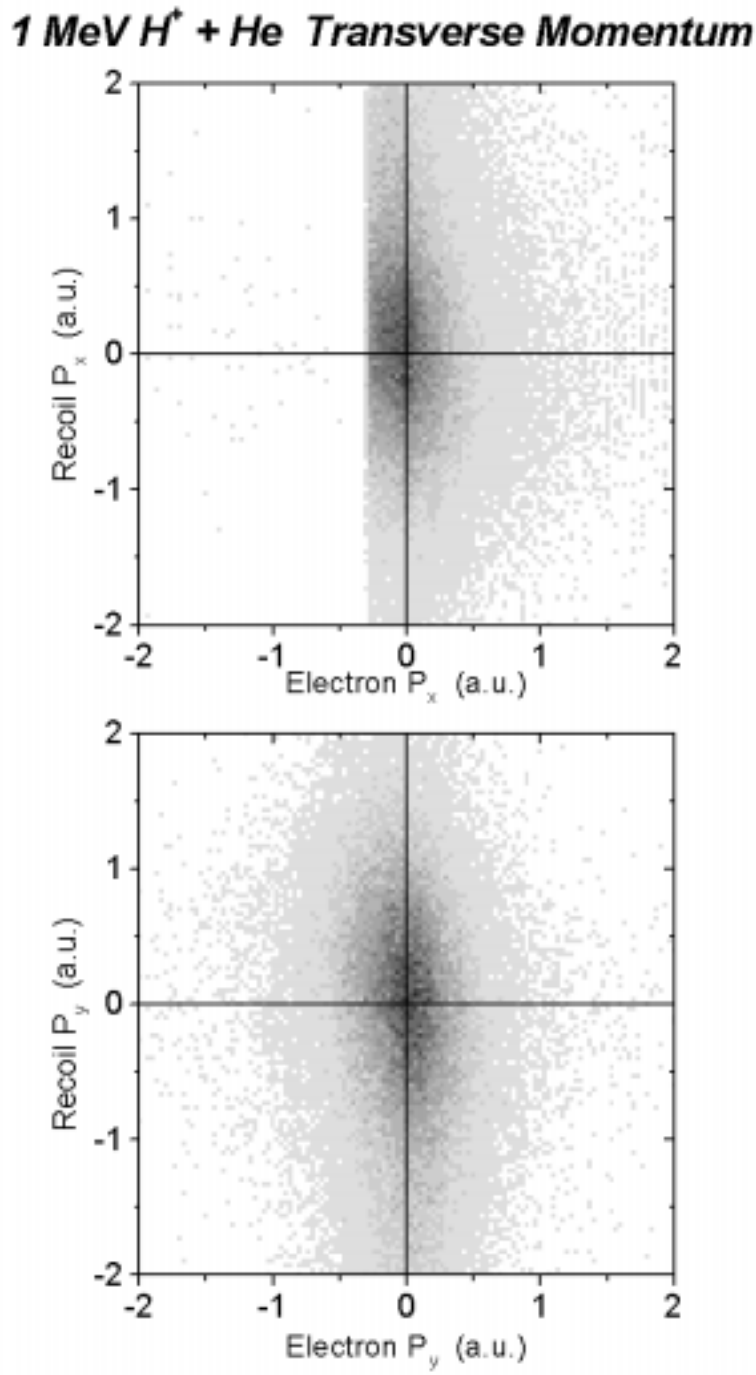

Figure 4.17: Density plots of the doubly differential cross sections $d^2\sigma/dP_{xe}\,dP_{xR}$ and $d^2\sigma/dP_{yR}\,dP_{ye}$ for the collision system 1 MeV H^+ + He.

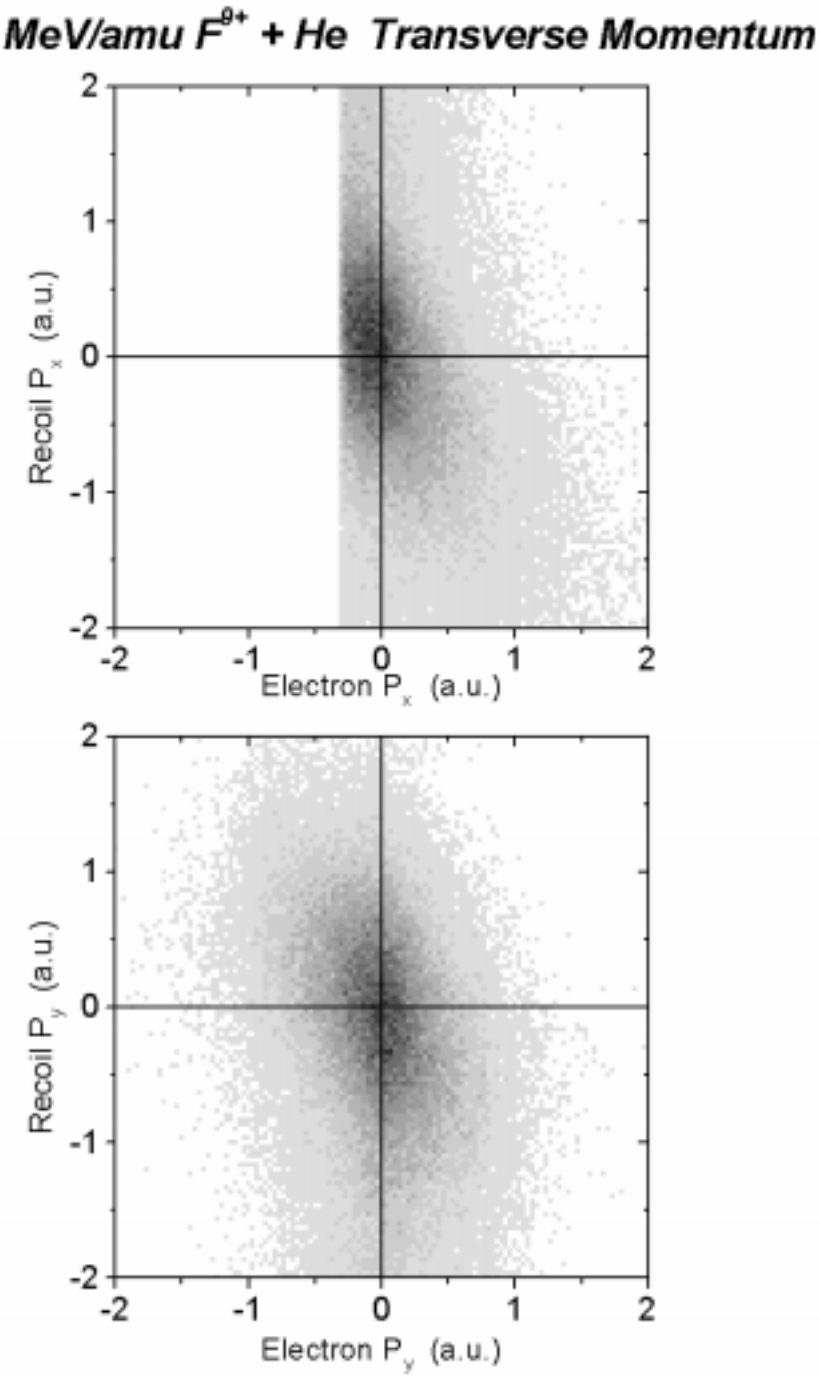

Figure 4.18: Density plots of the doubly differential cross sections $d^2\sigma/dP_{xe}\,dP_{xR}$ and $d^2\sigma/dP_{yR}\,dP_{ye}$ for the collision system 1 MeV/amu F^{9+} + He.

Transverse Momentum Coordinate System

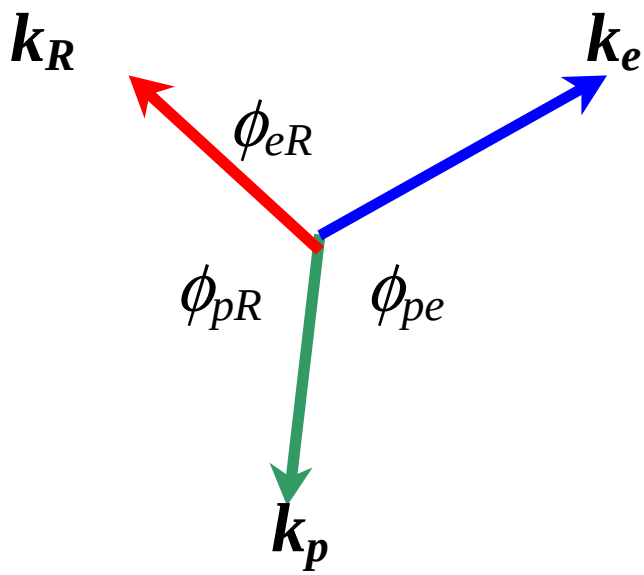

$\boldsymbol{k_R} = -\boldsymbol{k_e}$, ϕ_{eR} : *"Dipole or Photionization-Like"*
$\boldsymbol{k_e} = -\boldsymbol{k_p}$, ϕ_{ep} : *"Binary Encounter"*
$\boldsymbol{k_p} = -\boldsymbol{k_R}$, ϕ_{pR} : *"Nuclear"*

Figure 4.19: Vector diagram of transverse momenta in the plane perpendicular to the ion beam.

the collision systems measured, and therefore there must be additional momentum exchange involved.

To explore this idea further, we must introduce more complicated spectra. To aid the reader in visualization, figure 4.19 shows the three momentum vectors in the transverse plane. The angles between each pair of momentum vectors in the transverse plane provide useful parameters for analyzing the collision behavior. For example, if the scattering is purely binary encounter, then the corresponding angle between the electron and projectile (ϕ_{eP}) must be 180°. The same is true for nuclear and photoionization-like scattering, the relevant angles being ϕ_{eR} and ϕ_{PR} [4.11]. Figures 4.20-4.22 show the distributions in transverse angle for each of the collision systems. The density plot is a correlation diagram of ϕ_{PR} versus ϕ_{eR}. The correlation in this type of plot appears as follows:

1) Pure nuclear scattering appears as a concentration of counts along the top axis in the figure. This corresponds to ϕ_{PR} =180°.
2) Pure photoionization-like scattering appears as a concentration of counts along the left axis in the figure. This corresponds to ϕ_{eR} =180°.
3) Pure nuclear scattering appears as a concentration of counts along the 45° line connecting the upper left and lower right corners of the figure. This corresponds to ϕ_{eP} =180°.

In the three systems shown, there is no evidence from the density plot that any one scattering type dominates. In each case, there is a mix. As can be seen from the singly differential cross sections, the strongest scattering type in each case is nuclear. There is evidence of each type in all of the spectra, except for the 1 MeV proton case. Here we see that there is no preferential scattering for ϕ_{eR} =180°.

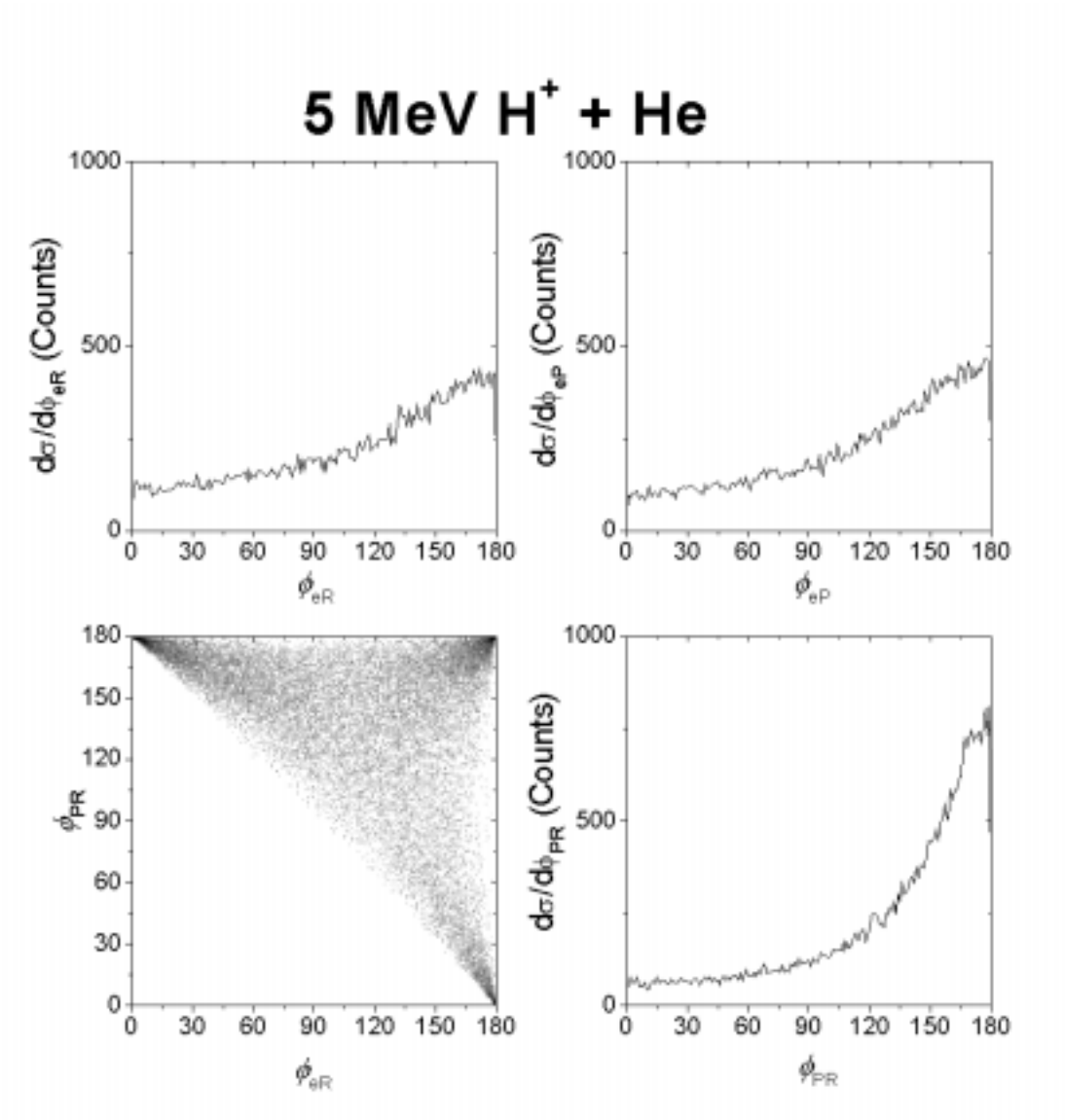

Figure 4.20: Distributions in transverse angle for 5 MeV H^+ + He. The density plot is the doubly differential cross section $d^2\sigma/d\phi_{PR}d\phi_{eR}$.

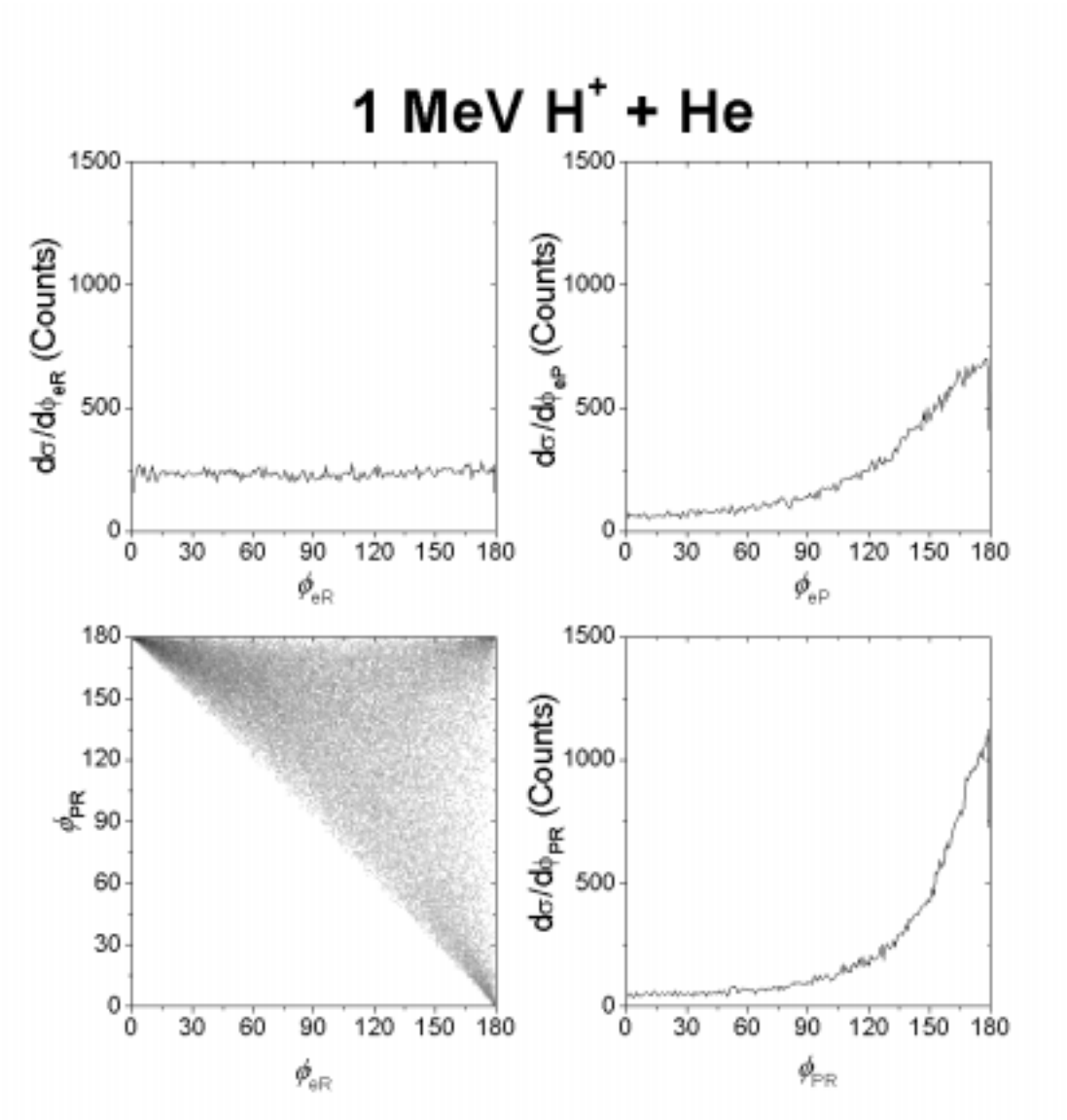

Figure 4.21: Distributions in transverse angle for 1 MeV H^+ + He. The density plot is the doubly differential cross section $d^2\sigma/d\phi_{PR}d\phi_{eR}$.

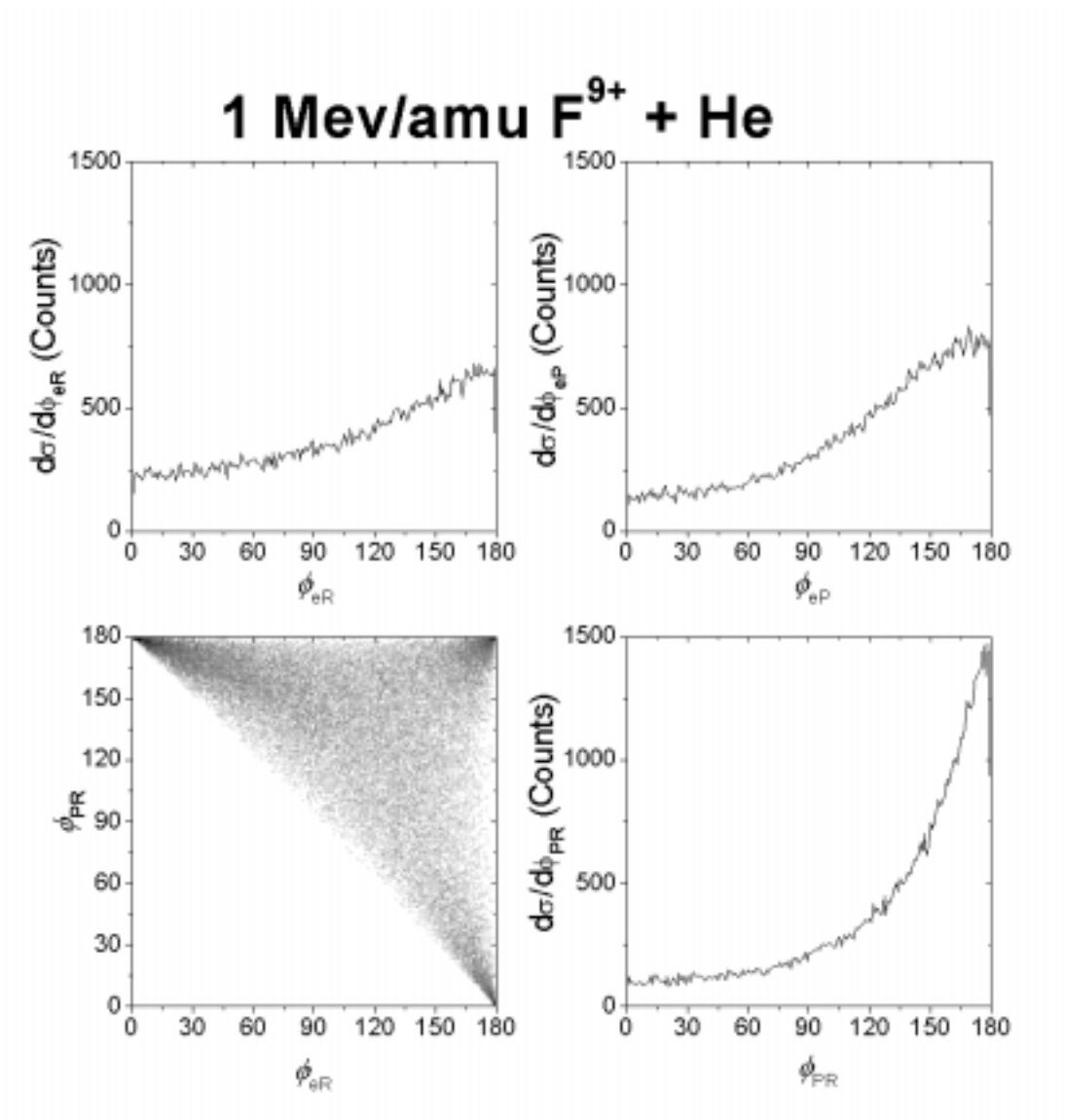

Figure 4.22: Distributions in transverse angle for 1 MeV/amu F^{9+} + He. The density plot is the doubly differential cross section $d^2\sigma/d\phi_{PR}d\phi_{eR}$.

One drawback to the plots of transverse scattering angle is that they do not show any possible dependence of the correlation on the relative magnitudes of the two transverse momentum vectors. In figures 4.23-4.25, we present a solution to this problem. These are density plots of the projection of vector "A" onto vector "B" versus vector "B" for all six combinations of vector pairs. As in the case of the other correlation plots, a line through the origin with a slope of –1 corresponds to a complete momentum balance between the two vectors. Let us take the example of the two plots found in the top row of each figure. The left graph is a density plot of the projection of the recoil transverse momentum vector onto the electron transverse momentum vector versus the magnitude of the electron vector:

$$d^2\sigma / dP_{\perp R}\, d(P_{\perp e} \cos(\phi_{eR})).$$

The right graph is a density plot of the projection of the electron vector onto the recoil vector versus the magnitude of the recoil vector:

$$d^2\sigma / dP_{\perp e}\, d(P_{\perp R} \cos(\phi_{eR})).$$

A correlation on either of these graphs would indicate photoionization-like scattering. We see more evidence of a strong nuclear correlation in all cases. The upper plots in the 1 MeV proton case clearly show a lack of correlation of the results in the case of photoionization like scattering

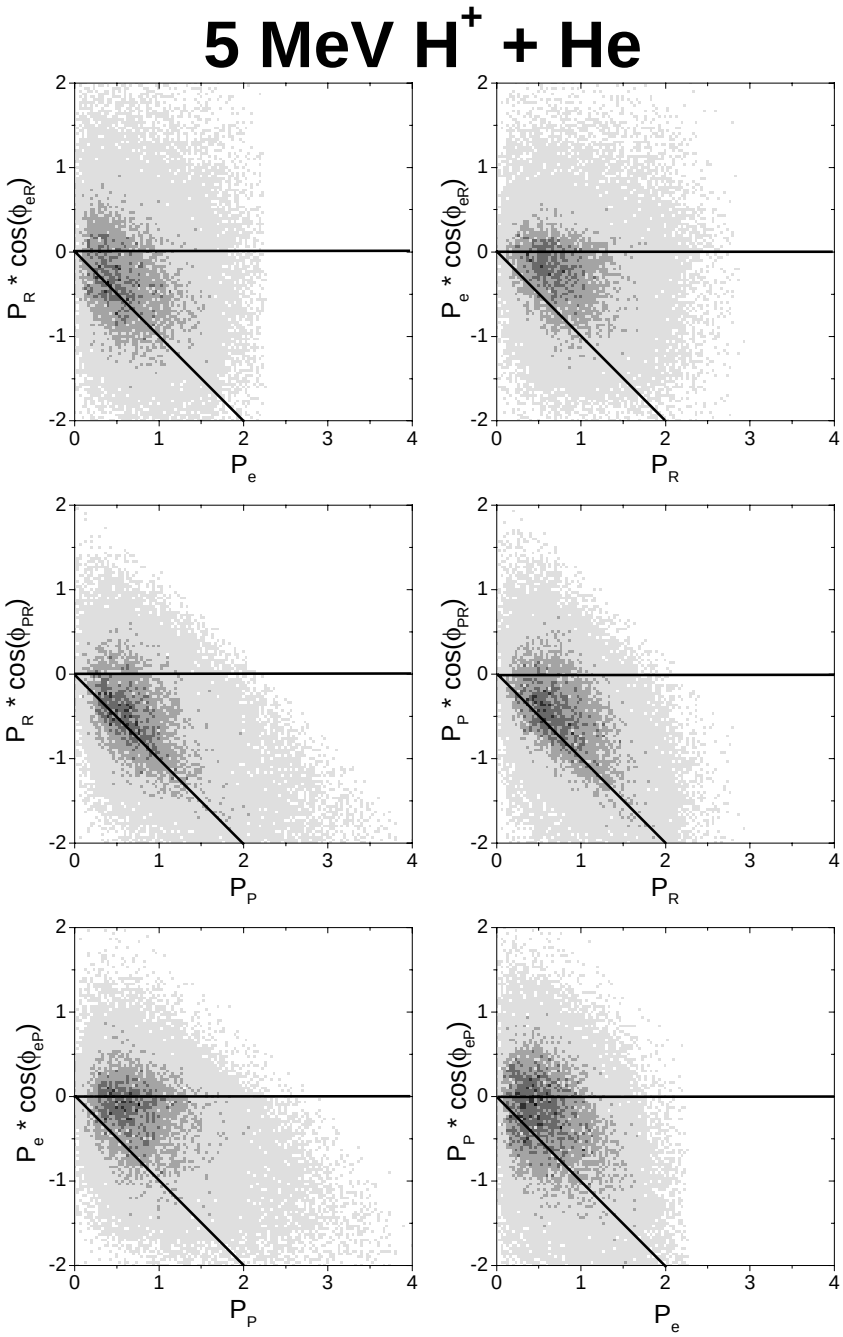

Figure 4.23: Density plots of the projection of vector "A" onto vector "B" versus vector "B" for all six combinations of vector pairs for the system 5 MeV H^+ + He. The density is proportional to the doubly differential cross sections $d^2\sigma / dP_{\perp i}\ d(P_{\perp j}\ cos(\phi_{ij}))$ where *i* and *j* are all combinations of *R*, *P*, and *e*. The diagonal lines represent the correlation between the two vectors.

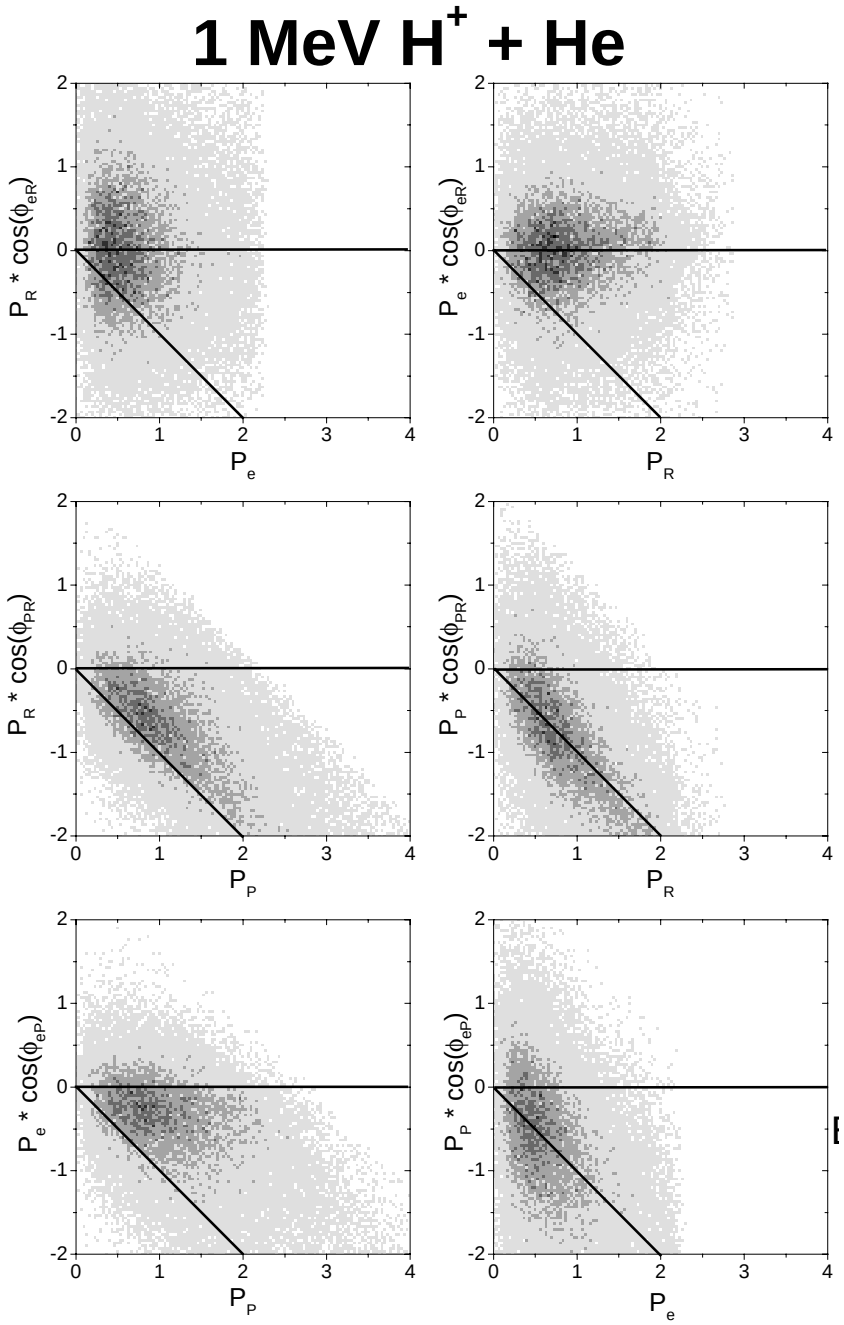

Figure 4.24: Density plots of the projection of vector "A" onto vector "B" versus vector "B" for all six combinations of vector pairs for the system 1 MeV H^+ + He. The density is proportional to the doubly differential cross sections $d^2\sigma / dP_{\perp i}\ d(P_{\perp j}\ cos(\phi_{ij}))$ where *i* and *j* are all combinations of *R*, *P*, and *e*. The diagonal lines represent the correlation between the two vectors.

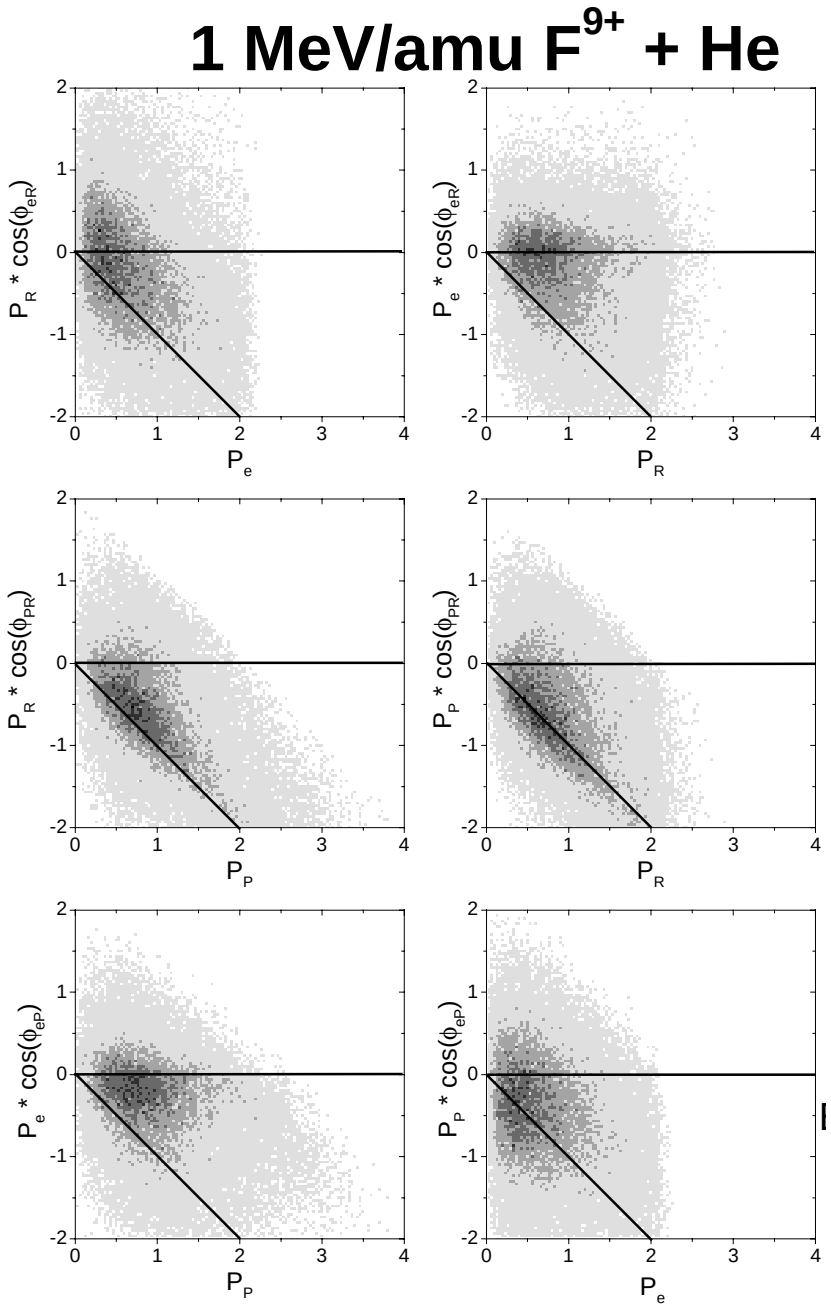

Figure 4.25: Density plots of the projection of vector "A" onto vector "B" versus vector "B" for all six combinations of vector pairs for the system 1 MeV/amu F^{9+} + He. The density is proportional to the doubly differential cross sections $d^2\sigma / dP_{\perp i}\ d(P_{\perp j}\ cos(\phi_{ij}))$ where *i* and *j* are all combinations of *R*, *P*, and *e*. The diagonal lines represent the correlation between the two vectors.

4.4.5 Discussion

In summary, we have measured the complete kinematic behavior for soft electron production in three collision systems with velocities from 6.3 a.u to 14 a.u. and charges of 1 and 9. We have derived the conservation laws for small momentum transfer, and separated the data into longitudinal and trasverse components. By taking a variety of views in the multidimensional phase space, we were able to discern the relative strengths of the two-body interactions.

In the longitudinal direction, the results are well understood. The electron and recoil momentum have a strong correlation as predicted by equation 4.7. The singly differential cross sections agree well with CDW theory. The strength of the post-collision interaction is also well predicted, with the higher charge having a greater effect.

In the transverse direction, there is evidence for two significant trends in the data. First, there is remarkably strong evidence for nuclear scattering in our data as compared to the results from the collision system 3.6 MeV/amu Se^{28+} + He. When early data showed this trend, we were skeptical of our results. A poor resolution in the recoil measurement could account for this effect, so we repeated the experiment with the careful calibrations described in appendix A.

The effect was confirmed and evident in the upper plot of figure 4.27. Shown are the distributions in ϕ_{PR} for each of the three present systems in addition to 2 MeV H^+ data from the early set of experiments. The data are normalized at low angles in

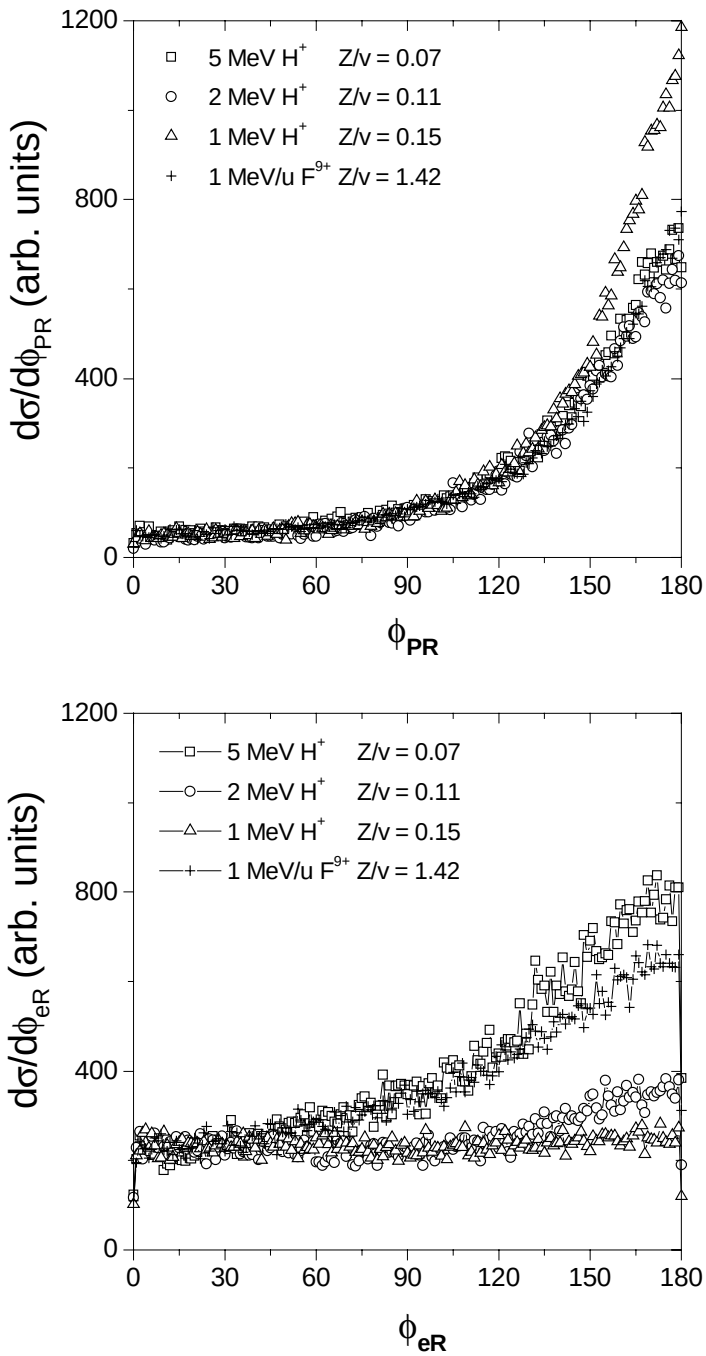

Figure 4.27: (Top): Distributions in the angle between transverse recoil and projectile momenta, indicating a strong nuclear scattering for each system. (Bottom): Distributions in the angle between transverse recoil and electron momenta. There is an apparent minimum in the varience with Z/v. In both plots, the data are normalized to match at small angles for comparison.

order to see the relative strength of the nuclear scattering for each system. Clearly, there is a strong preference for the recoil and projectile to scatter in opposite directions. The projectile charge to velocity ratio (Z/v) is the scaling parameter used for the majority of existing theory. However, in the case of the 3.6 MeV/u Se^{28+} data from Moshammer *et al*. [4.11], the value of this ratio is 2.3, and their results indicate a strongly photoionization-like behavior. For our measurements of the 1 MeV/u F^{9+} system, the ratio is 1.4, which is of comparable size. Yet our results indicate a strongly nuclear behavior. We must therefore conclude that either one of the measurements is in error, or the behavior is more complex than a simple Z/v dependence.

A similar plot for photionization-like scattering (ϕ_{PR}) is shown in the bottom plot of figure 4.27. The dependence on Z/v is clearly nonmonotonic, with an apparent minimum effect for the 1 MeV H^+ case. Data with a more continuous variation in Z and v are necessary to explore this effect further.